Causality-based mapping of functional pulmonary vascular networks

Amran K. Asadi
Department of Biomedical Engineering
University of California- San Diego
San Diego, CA 92121

Tatsuya J. Arai
Department of Biomedical Engineering
University of California- San Diego
San Diego, CA 92121

Abstract

'Granger' causality was explored as a method for determining effective/functional vascular connections between lung regions in a two-dimensional time series of blood flow MR images, generated using Arterial Spin Labeling (ASL). Two different approaches to segmentation were employed to attempt to optimize the ratio of spatial to temporal data, lobar segmentation and 'high-resolution' segmentation of the lung field. While lobar segmentation yielded significant causal interactions during data collected in normoxic breathing, insufficient number of observations hampered detection causal interactions during either hypoxia or hyperoxia. In contrast, utilizing higher resolution segmentation on data acquired at twice the temporal resolution (5s as opposed to 10s), significant differences in effective network connectivity and flow autonomy were revealed. Network connectivity and autonomy were enhanced during hypoxic breathing compared to normoxia or hyperoxia, suggesting a level of active flow control present in the healthy lung that becomes engaged when oxygen levels are reduced.

1 Introduction

'Granger' causality or Granger causal methods describe an array of statistical and analytical techniques that attempt to elucidate the directed flow of information between a set of observed time-varying signals using the idea of temporal precedence. Although having its origin in economic theory [1], these techniques have found a myriad of applications in the field of neuroscience, where understanding network causal dynamics is of particular import. In combination with functional magnetic resonance imaging (fMRI), there now exists a framework for the investigation of complex and rapidly adapting neural networks in humans that possesses both spatial and temporal specificity. For example, Deshpande et al incorporated a causal analysis of fMRI data to successfully demonstrate changes in neural network connectivity concomitant with motor fatigue [2]. In another study, Roebroeck et al. applied similar methodology to the mapping of interactivity between brain regions during complex visuo-motor tasks [3]. While these examples highlight application to in-vivo neural networks, the techniques employed are neither limited to the brain, nor neural networks themselves. We seek to extend the scope of these techniques to the purpose of studying vascular dynamics in the human lung.

1.2 The pulmonary vascular network

Efficient gas exchange is of primary importance in the lung. Whereas on first pass this may be thought to result solely from passive diffusion processes, in reality the relative effectiveness of passive diffusion depends heavily upon proper micro and macro-scale matching of flow between two distinct mechanical networks (the exchanger mass-transport problem). Furthermore, evidence exists to suggest that there is a strongly active and temporally varying component to vascular network regulation in the healthy lung [4]. Hypoxic pulmonary vasoconstriction (HPV), a phenomena that results in reduced blood flow to poorly ventilated lung regions [5], may serve as an important mechanism by which this regulation occurs.

The pulmonary vasculature is particularly well suited to the application of network analysis. As the entirety of cardiac output travels through the pulmonary vascular bed, local changes in vessel resistance by necessity must affect flow in other, potentially more distant regions, a phenomenon termed 'flow steal.' Yet, as the matching of ventilation and perfusion at the small scale uniquely determines alveolar oxygen pressure (assuming constant inspired concentration), the same HPV mechanism described earlier has the potential to drive the emergence of complex flow feedback dynamics across the organ as a whole. As most lung pathology has as its hallmark a disruption of vascular and ventilatory coupling, the possibility exists that quantifying disruption in, or alteration of, vascular network dynamics may provide diagnostic utility, with the hope of early identification of progressive disease before changes in gross pulmonary function can occur.

1.3 Non-invasive quantification of flow

While network analysis of the kind described above is certainly not a new idea, it is only relatively recently that methodological developments have permitted the acquisition of spatially and temporally detailed information on blood flow in the human lung. Prior studies in this field have, for example, utilized microsphere tracer methods in which radiolabeled microspheres delivered intravenously embed themselves in pulmonary capillaries in proportion to local flow [6-9]. Not only are number of temporal observations limited to the number of different labels available, but the technique further requires animal sacrifice to count the number of embedded microspheres, making translation to human study impossible. Radiation exposure and contrast toxicity severely hampers repeated use of X-ray, CT and other fluoroscopic techniques to the acquisition of blood flow data over time, making these poor choices for studying pulmonary vascular temporal dynamics in any meaningful way.

While MRI is often thought of in terms of purely anatomical imaging, a significant interest has developed in utilizing the underlying physical properties of the technique to capture 'function' as opposed to anatomy. A recent adaptation, known as pulmonary Arterial Spin Labeling (ASL), allows the repeated creation of flow image contrast with temporal resolution on the order of 5-10s and spatial resolution of 1 cm^3 [4, 10, 11].

1.4 Application of Granger causal analysis

Now with the capability to acquire spatio-temporal blood flow measurements, the challenge arises as to how best to leverage these complex data sets to begin to ask physiologically meaningful questions about the mechanisms that underlie blood flow heterogeneity in the lung, and how it relates to proper gas exchange function. To this end, it is believed that the framework of Granger causality discussed in the context of neural networks above provides a potential means. It is hypothesized that, when faced with a hypoxic challenge, the pulmonary circulation actively responds in an effort to maintain gas exchange efficiency, and further, that this response may be characterized by an enhancement of effective connectivity between lung regions as blood flow is purposefully redistributed in both a dynamic and coordinated fashion. As a corollary, it is further supposed that at rest or when faced with supplemental oxygen, the healthy lung is largely in a state of 'weak' control characterized by uncoordinated activity.

2 Methods

2.1 Pulmonary arterial spin labeling (ASL)

Arterial spin labeling is the one of magnetic resonance imaging techniques, which quantifies the spatial distribution of pulmonary blood flow. The essential idea of the technique is that the incoming blood from outside of image slice is magnetically manipulated and thus highlighted in the inside of image slice. For imaging of lung, flow-sensitive alternating inversion recovery with an extra radiofrequency pulse (FAIRER) is used. This technique acquires two MR images in series; For the first image, a slice-selective inversion recovery preparation pulse is applied to a band that encompasses the imaging slice. The magnetization within a slice is inverted, while the magnetization outside the slice is unchanged. After a delay time (T_I), an image is acquired. The measured net MR signal in a voxel is a mixture of signals of static pulmonary tissue in the voxel, which are inverted, and the signals of delivered blood, which are not inverted. For the second image, the inversion recovery preparation pulse is applied non-selectively so that tissue and blood magnetization in both inside and outside of image slice are all inverted. After the same delay time (TI), the obtained net MR signal in a voxel is a mixture of signals of static tissue and delivered blood, which are both inverted. When two images are subtracted, the signals from static tissue within a slice is canceled. However, the signal of blood delivered is not canceled, leaving a difference signal, which is proportional to the delivered blood volume during the delay time (TI).

2.2 Respiratory gating and imaging

MR image was acquired during a short breath-hold at functional residual capacity (FRC) lung volume. The image acquisition was repeated approximately every 5 seconds, altering between two types of ASL images. Between two consecutive image acquisitions, subjects were asked to complete one breathing cycle and repeat FRC volume for another image acquisition. Each experimental run covers 300 MR images in ~25 minutes so that 150 pulmonary blood flow images were computed for each subject.

2.3 Experimental design

Each subject underwent studies (Normoxia, Hypoxia, and Hyperoxia) with challenge blocks of altered FIO2 in randomized order between subjects. Each run consists of three challenge blocks: 100 breaths (images) on ambient air (FIO2 = 0.21), 100 breaths on the test gas from the bag, followed by another block of ambient air. Thus, 50, 10, and 40 pulmonary blood flow images were obtained during the first block, transition between ambient air and test gas, and test gas, respectively

2.4 Granger causality and autonomy

Granger causality implements a statistical interpretation of causality where time series Y Granger causes X if knowing the past of Y can help to predict X, better than knowing the past of X alone. The Granger causality uses an autoregression model, with the number of lagged values to include determined by application of an appropriate criteria (either Akaike or Bayesian information criterion). Let x and y be time series X and Y respectively, and x is expressed as autoregression of proper lagged values of x and u1 is residual (Eq.1). This is an autoregression prediction model.

$$x_t = \sum_{s=1}^{\infty} E_{1s} x_{t-s} + u_{1t}$$

$$var(u_{1t}) = \Sigma_1$$

Here, the variance of vector u_1 is Σ_1.

$$x_t = \sum_{s=1}^{\infty} E_{2s} x_{t-s} + \sum_{s=1}^{\infty} F_{2s} y_{t-s} + u_{2t}$$

The term of lagged values of y is added to the autoregression and residual u_2 is computed.

$$var(u_{2t}) = \Sigma_2$$

The variance of vector u_2 is Σ_2.

$$\ln (|\Sigma_1|/|\Sigma_2|)$$

If Σ_2 is reduced by adding the past of Y and the log of the ratio of two variances (Eq.3) is positive suggesting the autoregression prediction model is improved, Y "Granger causes" X.

$$y_t = \sum_{s=1}^{\infty} G_{1s} x_{t-s} + v_{1t}$$

$$var(v_{1t}) = \mathrm{T}_1$$

$$y_t = \sum_{s=1}^{\infty} G_{2s} x_{t-s} + \sum_{s=1}^{\infty} G_{2s} y + v_{2t}$$

$$var(v_{2t}) = \mathrm{T}_2$$

$$\ln (|\mathrm{T}_1|/|\mathrm{T}_2|)$$

Granger autonomy is understood as the degree of self-causation. Instead of asking whether the prediction error of X is reduced by including past history of Y, the Granger autonomy measure asks the other way around: the prediction error of Y is reduced by inclusion of its own past, given a set of external variables X_1, $X_2 \ldots X_n$.

2.5 Application to the vascular network

2.5.1 Lobar segmentation

A pulmonary blood flow image was divided into three parts based on the three anatomical lobes in the right lung (Figure ##). The mean blood flow value within each lobe was computed for each image so that three time series data were obtained for each subject; 3 variables and 150 observations. G-causality and G-autonomy among three time series data were then computed, respectively. The false discovery rate for multiple testing was set at 5% for statistical significance.

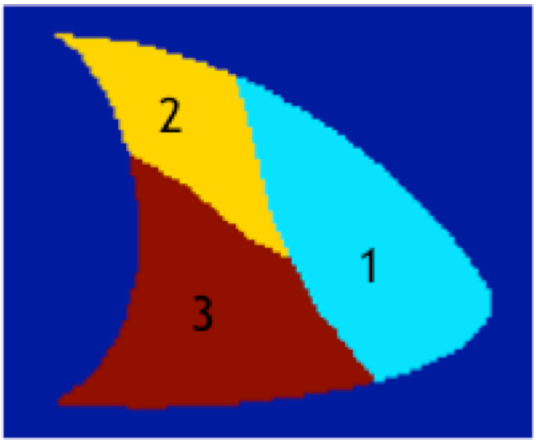

Figure 1. Three lobes in the right lung.

In a sagittal slice of right lung with spine posture, three lobes are distributed in over six

2.5.2 High-resolution segmentation

A pulmonary blood flow image originally acquired at 256x128 with a 40cm field of view (yielding 1.5 mm x 3 mm x 10 mm) was spatially smoothed using a gaussian kernel, providing spatial downsampling to 32x32. In contrast to the data utilized for lobar segmentation, data acquisition for the high-resolution segmentation protocol was conducted utilizing a 5-second temporal resolution and 180-breath runs on a single gas (i.e. all air, all hypoxia, or all hyperoxia). A region of interest outlining the lung field was taken, and edges of the lung field were discarded to prevent partial voluming effects, yielding approximately 40 individual voxel time series within the sagittal slice as shown in Figure 2 below. The G-causality matrix and G-autonomies were computed on these voxel time series for the hypoxic, hyperoxic, and normoxic periods separately for comparison. As before, the FDR was set to 5% to adjust for multiple comparisons. Autonomy values deemed significant were then summed to yield an overall measure of 'lung autonomy' for each condition.

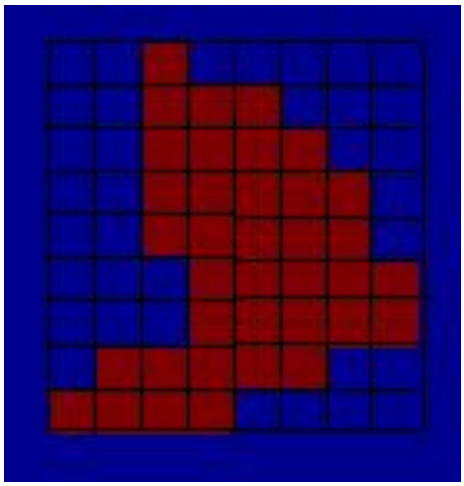

Figure 2. High-resolution segmentation of sagittal slice through the right lung

3 Results

3.1 Lobar interactions

For normoxic challenge using all 150 pulmonary blood flow images, Granger causality and autonomy were both discovered except for Subject D (Table 1.). In five subjects, inferior lobe (#3 in Fig. 1) had a tendency to show both causality (either source or sink) and autonomy. The results from hypoxic and hyperoxic (using 40 pulmonary blood flow images) failed to reject null hypotheses for both causality and autonomy, respectively.

Table 1. Granger Causality and Autonomy among three lobes in right lung during Normoxia

Subject	Causality	Autonomy
A	**X**	3
B	3➔1	3
C	2➔3	1 and 3
D	**X**	**X**
E	3➔1	2 and 3
F	1➔3	1, 2, and 3

The false discovery rate for multiple testing was set at 5% for statistical significance. Granger causality: the arrow ➔ represents the causal flow, i.e. 3➔1: lobe #3 causes lobe #1. **X** failed to reject null hypothesis. 1: superior lobe, 2: middle lobe, and 3: inferior lobe, respectively.

As seen in Table 1, there was a trend that inferior lobe (#3 in Fig. ##) showed both causality (either source or sink) and autonomy in five subjects, suggesting there is an active regulation controlling the blood flow in the lobe. Both hypoxic and hyperoxic runs failed to reject null hypotheses, implying that 40 observation is not enough to discover either causality or autonomy.

3.1.1 Individual voxel interactions

Data from two subjects were analyzed utilizing G-causality and G-autonomy measures for each of three conditions; air breathing, hypoxic (12.5% Oxygen) breathing, and hyperoxic (100% Oxygen) breathing. Figure 3 displays the G-causality matrices for each of these conditions for one subject.

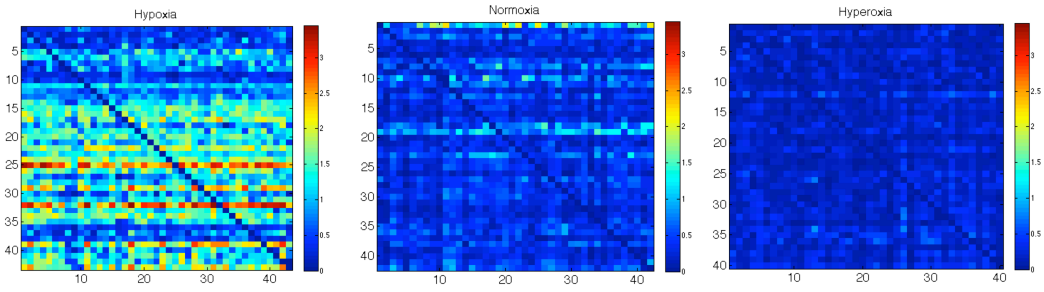

Figure 3. Granger causality matrices for subject A in hypoxia (at left), normoxia (center) and hyperoxia (right).

Setting the FDR to 5% and analyzing for significant interactions for both subjects reveals the network topologies shown in Figure 4 for subject A, and Figure 5 for subject B.

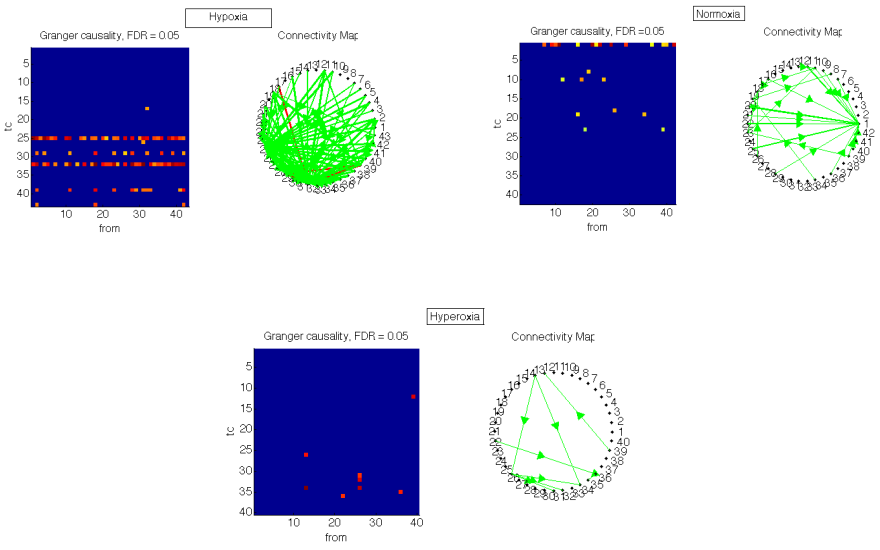

Figure 4. Significant causal interactions for subject A in hypoxia (top left), normoxia (top right) and hyperoxia (bottom). The FDR for multiple comparisons testing was set to 5%.

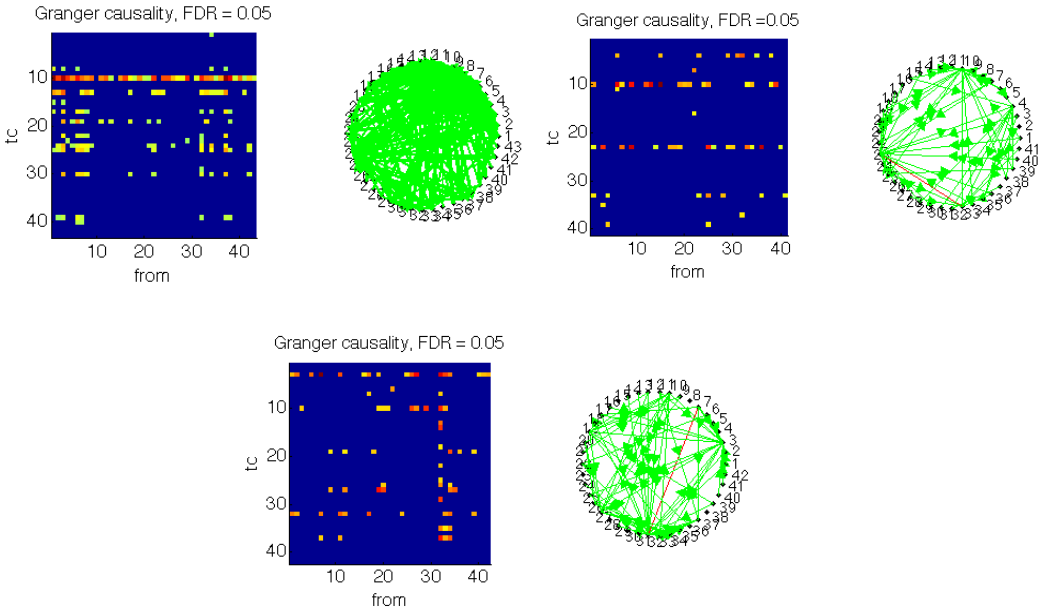

Figure 5. Significant causal interactions for subject B in hypoxia (top left), normoxia (top right) and hyperoxia (bottom). The FDR for multiple comparisons testing was set to 5%.

It can be clearly seen in both Figure 4 and Figure 5 that effective connectivity is the greatest in the hypoxic breathing condition, and reduced in either normoxic or hyperoxic breathing. Furthermore, at least in the case of subject A, it appears that there is a progressive decrease in connectivity as inhaled oxygen concentration increases. Summing significant autonomies for each of the conditions yielded (in order of hypoxia, normoxia, hyperoxia) 5.47, 1.4, and 0 for subject A and 3.21, 1.98 and 1.37 for subject B. These changes reflect a decrease in the influence of past values of flow to individual lung regions on future values of flow to those same regions as oxygenation increases. It should be noted that this does not necessarily reflect that flow is more stable during hypoxia, but that changes in flow become more predictable concomitant with activation of hypoxic pulmonary vasoconstriction, and less so as HPV is reduced.

4 Conclusions

As a first foray into the application of causality measures as a means of defining vascular network topologies, these data serve to underscore the potential for gaining powerful insight into the activity of complex physiologic feedback control when faced with environmental challenge. The data clearly demonstrate both enhanced connectivity and autonomy, which are indicative of an increasingly driven system, when faced with oxygen deficit known to be sufficient to induce active mechanisms of blood flow redistribution. Further, the data on autonomy also suggest that in healthy subjects breathing air, the pulmonary vasculature is largely in a state of weak control, which may further yet relax when oxygen becomes overly abundant. This may serve as an incredibly powerful potential tool for diagnosis and staging of clinical lung pathology that serves to disrupt mechanisms of ventilation and perfusion matching necessary for the maintenance of normal gas exchange. Should disruptions in these mechanisms be detectable via a similar analysis to the one presented herein, before changes in gross pulmonary function were to occur (i.e. decreases in blood oxygen saturation or spirometry), more advanced treatment regimens may be deployed at an earlier stage, slowing disease progression. Such advance warning signs detectable by causal analysis may be interpreted through an enhanced state of vascular effective connectivity at rest compared to normal subjects.

A significant challenge to application of causal techniques to these data sets lay in the general imbalance between the level of spatial resolution required to detect meaningful changes in flow, and the number of temporal observations available. Clearly, the lack of significant findings relating to hypoxia and hyperoxia vs the positive connections shown in normoxia for the lobar analysis suggests either insufficient temporal sampling, a general loss of information relating to over-smoothing in the spatial domain, or both. Future data acquisition must take this careful balancing into consideration, with at least 200 independent temporal measures of flow in each of the three conditions.

References

1. Granger, C.W.J., *Investigating Causal Relations by Econometric Models and Cross-spectral Methods*. Econometrica, 1969. **37**(3): p. 424-438.
2. Deshpande, G., et al., *Multivariate Granger causality analysis of fMRI data.* Human Brain Mapping, 2009. **30**(4): p. 1361-1373.
3. Roebroeck, A., E. Formisano, and R. Goebel, *Mapping directed influence over the brain using Granger causality and fMRI.* Neuroimage, 2005. **25**(1): p. 230-242.
4. Asadi, A.K., et al., *Spatial-temporal dynamics of pulmonary blood flow in the healthy human lung in response to altered FIO2.* Journal of Applied Physiology, 2012.
5. Dumas, J.P., et al., *Hypoxic pulmonary vasoconstriction.* General Pharmacology: The Vascular System, 1999. **33**(4): p. 289-297.
6. Glenny, R., et al., *Gravity is an important but secondary determinant of regional pulmonary blood flow in upright primates.* J Appl Physiol, 1999. **86**(2): p. 623-32.
7. Glenny, R.W., *Blood flow distribution in the lung.* Chest, 1998. **114**(1): p. 8S-16S.
8. Glenny, R.W., S. McKinney, and H.T. Robertson, *Spatial pattern of pulmonary blood flow distribution is stable over days.* Journal of Applied Physiology, 1997. **82**(3): p. 902-907.
9. Glenny, R.W., et al., *Temporal heterogeneity of regional pulmonary perfusion is spatially clustered.* J Appl Physiol, 1995. **79**(3): p. 986-1001.
10. Bolar, D.S., et al., *Quantification of regional pulmonary blood flow using ASL-FAIRER.* Magnetic Resonance in Medicine, 2006. **55**(6): p. 1308-1317.
11. Levin, D.L., et al., *Changes in pulmonary blood flow heterogeneity measured with ASL-FAIRER in asymptomatic smokers and patients with COPD.* International Society for Magnetic Resonance in Medicine, 12th Scientific Meeting and Exhibition, 2004: p. 180.